Journal of Catalysis 368 (2018) 31–37

Contents lists available at ScienceDirect

Journal of Catalysis

journal homepage: www.elsevier.com/locate/jcat

Dissolution of CoCu catalyst step defects by Co subcarbonyl formation

Greg Collinge [a], Norbert Kruse [a,c,d,*], Jean-Sabin McEwen [a,b,c,d,e,*]

[a] The Gene & Linda Voiland School of Chemical Engineering and Bioengineering, Washington State University, Pullman, WA 99164, USA
[b] Department of Physics and Astronomy, Washington State University, Pullman, WA 99164, USA
[c] Department of Chemistry, Washington State University, Pullman, WA 99164, USA
[d] Institute for Integrated Catalysis, Pacific Northwest National Laboratory, Richland, WA 99352, USA
[e] Department of Biological Systems Engineering, Washington State University, Pullman, WA 99164, USA

ARTICLE INFO

Article history:
Received 8 June 2018
Revised 6 August 2018
Accepted 10 August 2018

Keywords:
CoCu catalysts
CO hydrogenation
Nanoparticle reconstruction
Carbonyl formation
Step sites

ABSTRACT

In CoCu-based Fischer-Tropsch catalysis, the as-prepared nanoparticles, if allowed to self-assemble, exhibit a Co@Cu core-shell morphology that would render the catalyst inactive for CO hydrogenation. Therefore, a chemical reconstruction has to occur to create the catalytically active phase. While some of the thermodynamically-imposed driving forces for reconstruction have been identified and kinetic mechanisms experimentally probed, a thorough theoretical understanding on the molecular events has yet to be developed. Here, we employ a first-principles statistical mechanics approach to show that the reconstruction of CoCu in CO atmospheres is likely accomplished via subcarbonyl (multiple bonded CO) formation at the step and kink sites of CoCu catalysts. We find that the CO-induced antisegregation of subsurface Co atoms to step sites and the subsequent rupturing of Co subcarbonyls from these sites is thermodynamically feasible under experimentally-relevant CO pressures and temperatures. The results suggest that Co tricarbonyl formation along with its rupturing and diffusion onto the terraces is responsible for reconstruction. These Co tricarbonyls are shown to favorably dimerize, suggesting a potential route for nanoisland formation and morphological changes. Our results illustrate a strong correlation to surface carbonyl and inorganic complex chemistry of Co metal.

1. Introduction

Surface reconstruction is a reaction phenomenon known to alter the activity and selectivity of catalyst particles. Seminally, Leidheiser and Gwathmey [1] and later Schmidt and coworkers [2–4] were among the first authors showing that metal surfaces may either suffer chemically-induced (chemical) or thermally-induced (mechanical) reconstruction. A heavily studied example that demonstrates the differences between the two cases is the "(1×2) missing row reconstruction" of a clean Pt(1 1 0) single-crystal surface [5,6] in which every second row of atoms along the $[1\ \bar{1}\ 0]$ direction is missing. Exposing a (1×2) Pt(1 1 0) crystal surface to CO inverts the reconstruction process and reestablishes the bulk-truncated (1×1) form through a homogeneous nucleation process in which atoms move over a few lattice sites [7–9]. Chemical processes were thereafter shown to play a large role in the reconstruction of many single-crystal systems and typically employed STM (Scanning Tunneling Microscopy) and LEED (Low Energy Electron Diffraction) methods to observe these phenomena [10–18]. In terms of nanoparticles, FIM (Field Ion Microscopy) was shown to be a viable methodological approach since the field emitter samples used in FIM largely resemble a single, hemispherically-shaped, nano-sized catalyst particle. Local reconstructions of small-size facets were observed using FIM and proved the validity of the approach [19,20]. Importantly, a CO-induced morphological reconstruction of transition metal particles toward a cubo-octahedral shape was imaged with atomic resolution [21–23]. In the case of Ni and Rh field emitters, the morphological reshaping was correlated with the formation of $Ni(CO)_x$ [24] and $Rh(CO)_x$ ($x = 1–3$) [23,25], respectively, using atom-probe mass spectroscopy. IR (Infrared) and/or Extended X-ray Absorption Fine Structure (EXAFS) measurements with supported Ni [26] and Rh [27–30] nano-sized particles provided additional information on the mobility of high-index subcarbonyl species. Due to their mobility, they may ultimately cause the dissolution of the nanoparticles. In other cases, including Fischer-Tropsch active Ru and Co metals, no such dissolution occurred despite subcarbonyls being detectable in considerable amounts [31,32]. STM and atom probe mass

* Corresponding authors at: The Gene & Linda Voiland School of Chemical Engineering and Bioengineering, Washington State University, Pullman, WA 99164, USA.
E-mail addresses: norbert.kruse@wsu.edu (N. Kruse), js.mcewen@wsu.edu (J.-S. McEwen).

https://doi.org/10.1016/j.jcat.2018.08.011
0021-9517/

spectrometry with either low-index Co single crystal surfaces [33] or Co field emitters [32], respectively, posited subcarbonyl species to be the source of surface reconstruction. Theoretically, however, these mechanistic propositions have yet to be directly supported and detailed to provide a sound picture of the reconstruction processes.

CO-induced nanoparticle reconstruction is a well-studied phenomenon in other metal systems with some notable recent reports on nanoparticle formation on Cu(1 1 1) [34] and Pt dimer stabilization on Pt/Fe_3O_4(0 0 1) [35] upon exposure to CO. We also note that the relevance of such reconstructions on bimetallic systems has been demonstrated both experimentally [36] and computationally [37].

We have been interested in Co and CoCu-based Fischer-Tropsch (FT) catalysts for some time. These metals have been experimentally shown to result in reconstruction and/or reconfiguration upon exposure to CO and H_2 under CO hydrogenation conditions [33,38–42]. While some of the thermodynamic driving forces for these phenomena have been explored for both Co [43] and CoCu [39,44], the processes responsible for reconstruction have yet to be theoretically elucidated. Based on the wealth of evidence presented in the aforementioned studies and the prediction of geminal di- and tri-carbonyls on CoCu surfaces [39,44], we hypothesize that the formation of *diffusive* (or "mobile") Co subcarbonyls is the means by which reconstruction occurs on CoCu nanoparticles. The formation of subcarbonyls has been demonstrated, but the experimental evidence cannot always distinguish between immobile (highly metal-bound) and mobile (minimally metal-bound) metal subcarbonyls. This study aims at identifying, using density functional theory (DFT) calculations and statistical mechanical methods, the parameter space under which carbonyl formation and therefore reconstruction is possible on CoCu catalysts. Carbonyl formation has long been assumed to involve kink sites under high coverages of CO since metal-metal bonds can be repetitively ruptured in such sites and therefore lead to a reconstruction of the surface. However, this does not exclude step sites (layer edges), which can also bind multiple CO molecules. We therefore begin our study with a stepped CoCu surface: Cu/Co(7 5 5). This surface has a long 6-atom (1 1 1) terrace and a 1 atom high (1 0 0) step and is ideal for testing the feasibility of geminal Co di-, tri-, and tetracarbonyl rupturing from CoCu step sites. We provide our DFT parameters and methods in the Supplemental Information (SI) along with a justification of the underlying model.

Supplementary data associated with this article can be found, in the online version, at https://doi.org/10.1016/j.jcat.2018.08.011.

2. Results

2.1. Adsorption trends with CO coverage

The maximum stoichiometry of CO adsorption on terrace sites is presumed to be one CO per site while the maximum stoichiometry on step sites is four CO per site. Here, we separate step coverage (θ_{st}) from terrace coverage (θ_t) and relate these to the total coverage (θ) through their (nominal) relative proportions ($\frac{1}{5}\theta_{st} + \frac{4}{5}\theta_t = \theta$). With this in mind, we compute CO adsorption energies on Cu/Co(7 5 5) at various coverages and configurations wherein we keep total coverage constant and vary the step coverage from 0.00 ML to its associated maximum step coverage. We also consider converting a step Co monocarbonyl to step Co dicarbonyl where possible. Figs. S2 and S3 show all six total coverages tested, which range from 0.050 ML to 0.400 ML (the maximum allowable for a final 2.00 ML step coverage with 0.00 ML terrace coverage). In all cases, we calculate the CO adsorption energy with CO in the gas phase and the clean, Cu-terminated Cu/Co(7 5 5) surface as reference. We note also that we treat the presence of CO at step sites as inducing Co/Cu antisegregation: nearby subsurface Co is swapped with the step site Cu of interest. No additional Co or Cu are added or removed in these systems, eliminating the need for a Co or Cu atom reference. This mimics experimental conditions where the Co and Cu nanoparticle concentrations are fixed after synthesis.

Remarkably, the energetic trends at each coverage are shown to be identical over all of the total coverages up to and including 0.200 ML (Figs. S4, 1-A, and 1-B): as CO molecules are moved from the terrace to the step and then converted to dicarbonyls, the adsorption energy is steadily increased. In fact, Co dicarbonyl formation is shown to be significantly more favorable than dispersing an equivalent amount of CO over the steps as Co monocarbonyls, which can be seen in Fig. 1A and B. At a step coverage of 2.00 ML (Fig. 1C), forming a higher concentration of dicarbonyls (one dicarbonyl on each step site) is no longer most favorable. Instead, a configuration wherein a dicarbonyl forms at every other step site with excess CO spilling over to the terrace sites is calculated to be the most favorable (Fig. 1C(ii)). The CO adsorption energy for each dicarbonyl is also shown to be identical (-1.43 ± 0.02 eV) up to 0.200 ML (Figs. S4, 1-A, and 1-B) indicating that lateral interactions between dicarbonyls are negligible up to this point. As such, if one assumes entropy contributions from the adsorbed CO are roughly

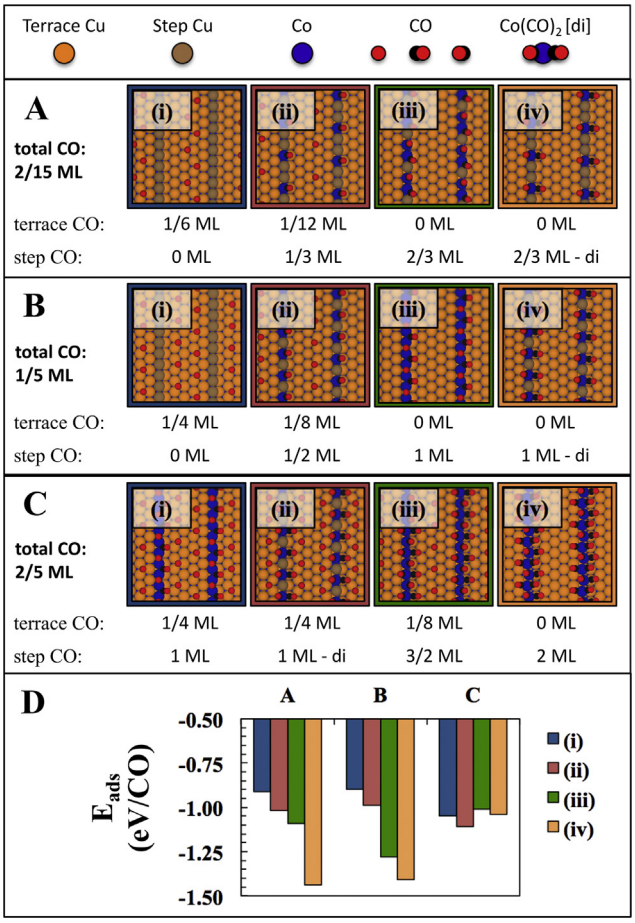

Fig. 1. CO adsorption energy of the three highest coverage systems tested: A, 2/15 ML, B, 1/5 ML, and C, 2/5 ML. The associated terrace and step coverages are shown below each structure. Panel D provides the calculated CO adsorption energy (in eV/CO) for each system, with bar graph colors corresponding to the color of each structure's border. In the associated top-down structures, the blue spheres are Co, the orange sphere are terrace Cu, the brown/olive colored spheres are step Cu, the black spheres are C, and the red spheres are O. See Figs. S2 and S3 for all systems tested.

equivalent, this result implies that a CO step coverage of *at least* 1.00 ML will be thermodynamically most favorable with a dicarbonyl configuration as shown in Fig. 1B(iv). All results considered, this also shows that dicarbonyl formation saturates at a step coverage of 1.00 ML. However, because we wish to investigate the possibility of rupturing higher index subcarbonyls, which are predicted to exist at high CO partial pressures [44], we move forward with a system that nominally represents a 0.67 ML step coverage of CO (see Fig. 1A(iv) as reference). This is an ideal model because the associated p(1 × 3) supercell is relatively small (computationally less burdensome) but still large enough to provide enough terrace space to more thoroughly test subcarbonyl formation at the step sites. We further note that because the energetics do not change as the supercell is decreased in its size along the direction parallel to the step edge (until the supercell is only 2 atoms long in that direction (Fig. 1C)), we do not expect that increasing the supercell size in this direction will change the results of this study.

2.2. Direct rupturing processes

Direct rupturing processes can be seen in Fig. 2A–C. The left structures depict the optimized initial states (IS) and the right structures the optimized final states (FS). Their DFT-based energy differences (ΔE) are summarized as the green solid line in Fig. 2G. As can be seen in Fig. 2G, direct metal-metal bond rupturing due to di- and tricarbonyl formation is very unfavorable (+1.72 eV and + 1.34 eV for the processes considered in Fig. 2A and B, respectively). Direct rupturing of the tetracarbonyl (Fig. 2C) is still found to be unfavorable (+0.47 eV) but is remarkably more favorable than the tricarbonyl rupturing process. This unfavorability, across all direct rupturing processes, is explained by further inspection of the FS of the direct rupturing processes (Fig. 2A–C): the process of rupturing creates an exposed Co atom, which we know is very unfavorable [39]. It is reasonable to assume this atom must be stabilized once exposed and this can be accomplished by re-formation of another geminal Co carbonyl which we will denote as the "kink-IS" (see the structures at the step edge of Fig. 2D–F). At this point, the kink-IS would be primed for another rupturing event. It is envisioned that kink site rupturing would be much more facile than the initial step site rupturing due to the lower number of metal bonds that must be broken to do so. Thus, step site geminal Co carbonyl rupturing would trigger a chain reaction of fast kink site rupturing events. This chain reaction of kink site rupturing events would continue until either the chemical potential of the subcarbonyls' ultimate FS reached that of the kink-IS, until another process like CO dissociation halts the process, or until newly-formed kink sites were exhausted. This latter possibility describes the effective dissolution of an entire step edge, which is necessary to explain the formation of cubo-octahedral particle shapes from spherical ones as observed earlier [21,23].

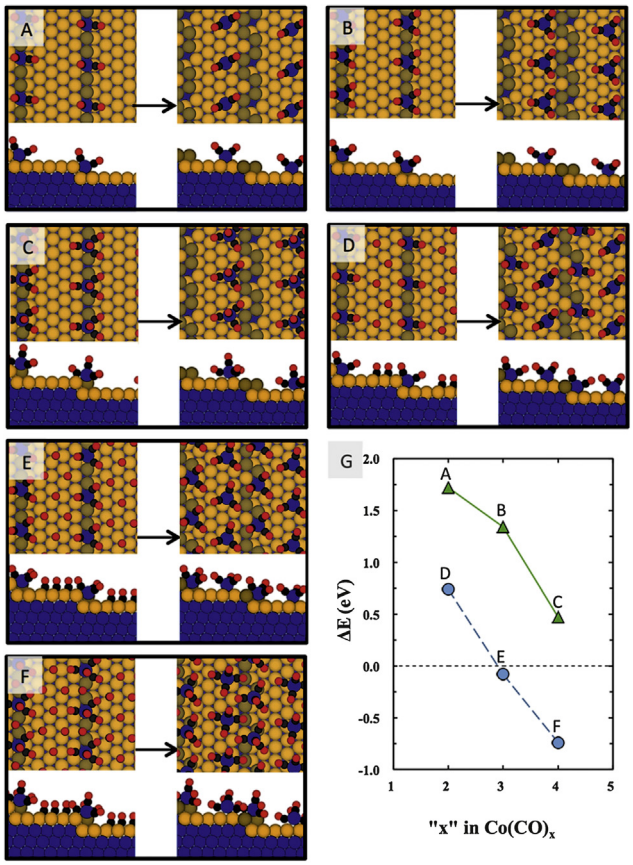

Fig. 2. (A–F) The six rupturing processes tested: direct rupturing of (A) a geminal Co dicarbonyl, (B) a geminal tricarbonyl, and (C) a geminal Co tetracarbonyl; rupturing and reformation of (D) a geminal Co dicarbonyl, (E) a geminal tricarbonyl, and (F) a geminal Co tetracarbonyl. The graph (G) shows the energy change for each of the (A – F) processes. The color scheme used here is identical to that of Fig. 1.

The dissolution of step and kink sites hinges on the favorability of reforming a new geminal Co carbonyl at the kink site in conjunction with the rupturing of the step Co. These kink-IS's can be seen in Fig. 2D–F, where only the necessary number of CO molecules that are needed to create the kink-IS are added to each system. Their ΔE's are represented in Fig. 2G as the dashed blue line. The geminal Co dicarbonyl (Fig. 2D) rupturing with the formation of the kink-IS is 0.74 eV lower in energy than the same system without the formation of the kink-IS, but it is still endothermic overall suggesting that this particular process is still unlikely. However, the geminal Co tricarbonyl (Fig. 2E) rupturing and kink-IS formation is essentially thermo-neutral (−0.08 eV) and the Co tetracarbonyl (Fig. 2F) is energetically well below the typical threshold for deeming a process favorable (−0.74 eV). It's important to note that this system seems sensitive to the choice of DFT functional. As can be seen in Fig. S3, the energy cost of rupturing appears to systematically raise if we switch to, for example, the vdW-DF functional. However, Table S2 shows that the vdW-DF functional increases the adsorption strength of CO on Cu/Co(7 5 5) despite the vdW-DF functional propensity to decrease it for Co(0 0 0 1) [45,46] and Cu(1 1 1) (we calculate E_{ads} with vdW-DF ∼−0.50 eV compared to E_{ads} with PBE ∼−0.80 eV). As such, the PBE functional was chosen in the present study because of the lower computed adsorption energy values on the Cu/Co(7 5 5) surface as compared to the corresponding vdW-DF functional values. For further information the reader is directed to the SI.

2.3. Thermodynamic stability of $Co(CO)_x$ at step and terrace sites

Interestingly, the IS and FS structures corresponding to the highly exothermic Co tetracarbonyl rupturing process (Fig. 2F: the brown lines in Fig. 3) are some of the *least* favorable structures when temperature and pressure are accounted for. This highlights the need for caution and diligence when evaluating the favorability of chemical processes based solely on DFT energies alone—the energy lowering effect observed can easily be an artifact of a highly unfavorable IS.

The lowest free energy structures at sub-ambient and ambient pressures in Fig. 3 are the step site geminal Co dicarbonyl (solid blue line) and step site geminal Co tricarbonyl (solid green line), both *without* nearby adsorbed CO. At the high pressures relevant to CO hydrogenation, Co tricarbonyl rupturing, represented by the red dashed line, becomes favorable only when the kink-IS is

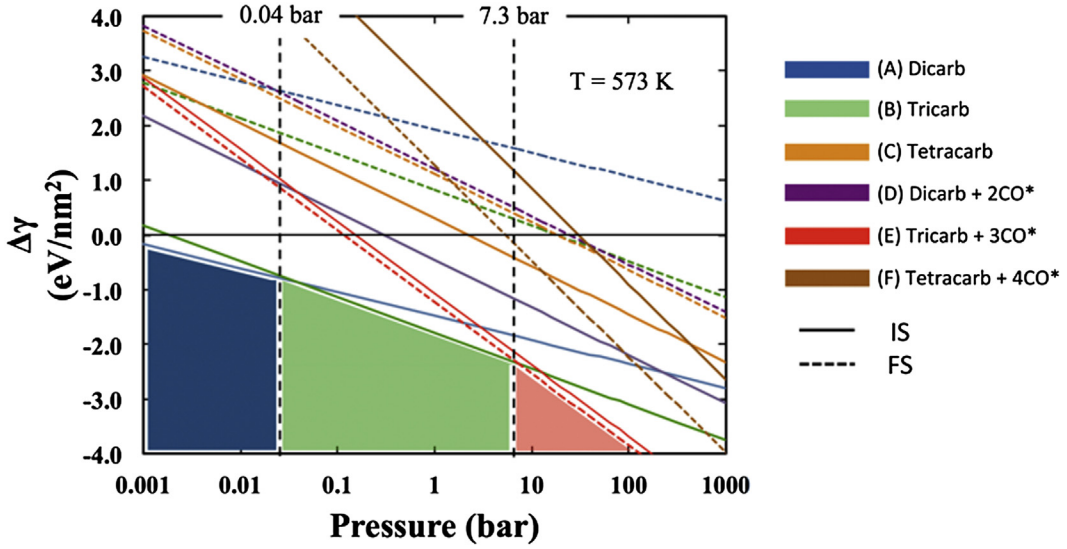

Fig. 3. Surface phase diagram of all structures shown in Fig. 2A–F. The vertical dashed lines denote a "phase change" and the corresponding pressure of the change is shown above them. Shaded regions help denote the lowest free energy structures: (from left to right) the Co dicarbonyl IS without nearby adsorbed CO (Fig. 2A: the left structure), the Co tricarbonyl IS without nearby adsorbed CO (Fig. 2B: the left structure), and the Co tricarbonyl FS with the kink-IS formed (Fig. 2E: the right structure).

formed (Fig. 2F: the FS). By utilizing Equation S1, we calculate the equilibrium constant between the initial geminal Co tricarbonyl and the final ruptured Co tricarbonyl (with the kink-IS formed) to be between ~6000 and ~50 in the 0.1–3.0 bar pressure ranges. This means that even given the errors inherent in the calculation of the exact free energies and thus propagated to the equilibrium constants (at 573 K, this error is roughly ±6 K_e given an approximate 0.2 eV free energy error), we can still expect there to be a non-negligible number of rupturing events at ambient pressures. Initial step-site rupturing events are expected to be the rate limiting step of the entire dissolution process as kink-IS's more easily rupture, and in this way facile restructuring of the CoCu catalyst would still be possible even at ambient pressures. It should be further noted that the vacancy left after tricarbonyl removal from the step would very likely be a site of high reactivity. However, it may be anticipated that kink site $Co(CO)_x$ would be even more favored than step site $Co(CO)_x$, especially at high coverages when steric effects come into play and thus competitive with other reactions that might take place at the vacancy. The repetitive removal (rupturing) of kink site $Co(CO)_x$ would then lead to the reconstruction of the surface, as shown for Ni and Rh [23,47], and likely to occur for other transition metals, including Co. For the interested experimentalist, relevant vibrational frequencies for the species listed in Fig. 2 have been extracted and summarized in Table S3.

2.4. Dimerization of $Co(CO)_3$: first steps in nanoisland formation

We further investigate the possibility of Co tricarbonyl dimerization once ruptured Co tricarbonyls are formed. This process is depicted in Fig. 4 where DFT energies relative to that of the initial state (Fig. 4A) are shown in the accompanying graph. Two stable states (Fig. 4A and B) are found as a newly ruptured Co tricarbonyl diffuses toward a previously ruptured Co tricarbonyl. This process is found to be essentially thermoneutral ($\Delta E_{rxn} \sim 0.00$ eV). From here, three possible final dimerized states were tested: dicobalt subcarbonyl complexes with 5, 6, and 7 CO adsorbed; corresponding to the dicobalt penta-, hexa-, and heptacarbonyls seen in Fig. 4C, D, and E, respectively. The dicobalt penta- and hexacarbonyl formations are uphill in energy by only 0.17 eV and 0.18 eV, respectively; while the dicobalt heptacarbonyl formation is uphill by 0.50 eV. Since dimerization will be accompanied by a translational/configurational entropy loss, it is not expected that the dicobalt hexacarbonyl will readily form. However, because a CO is kicked off when the dicobalt pentacarbonyl is formed, it is likely that there is an entropy *gain* as gas phase CO degrees of freedom are recovered. In fact, adding the DFT energy cost of CO desorption (~0.9 eV) to this process and accounting for the Gibbs free energy gain associated with gas-phase CO degrees of freedom from only rotations and translations (about −1.2 eV at 1 bar and 573 K), this process comes out to be roughly −0.1 eV exergonic. Being even more uphill in energy and having the exact opposite entropy argument as that of the dicobalt pentacarbonyl, the formation of the dicobalt heptacarbonyl is far too endergonic (roughly + 0.8 eV) to be feasible.

2.5. CO adsorption scan of the Cu/Co(7 5 5) terrace

To examine how our choice of a (7 5 5) facet with 6-atom long terraces approximates a (1 1 1) terrace, we perform a scan of the CO adsorption energy across the terrace as a function of distance from the step edge and present the results in Fig. 5. At roughly 4 Å from the edge (site 3), until roughly 9 Å from the edge (site 7), CO adsorption is essentially equivalent to adsorption on Cu/Co(1 1 1). Terrace sites 1, 2, 8, and 9 are actually higher in energy (i.e. weaker adsorption energy) than these (1 1 1)-equivalent sites. Sites 10 and 11 are formally step sites. In this study, all molecules adsorbed on the terrace have been kept as closely as possible to the (1 1 1)-equivalent sites. We note also that these results compare interestingly to similar lattice gas modeling and temperature programmed desorption work done by Payne and Kreuzer who implicitly assumed that all terrace sites of stepped surfaces, like the (7 5 5) surface, would be equivalent [48]. The results in Fig. 5 show that this is clearly not always the case. As such, because of the size of the Co subcarbonyls it is possible that the higher energy terrace sites could affect the results by destabilizing the subcarbonyls. Thus, we can assert that our results are at worst an underestimate of the thermodynamic stability of the ruptured adsorbates and increasing the length of the terrace would at best increase the stability of adsorbed Co subcarbonyls and associated dimers, trimers, etc.

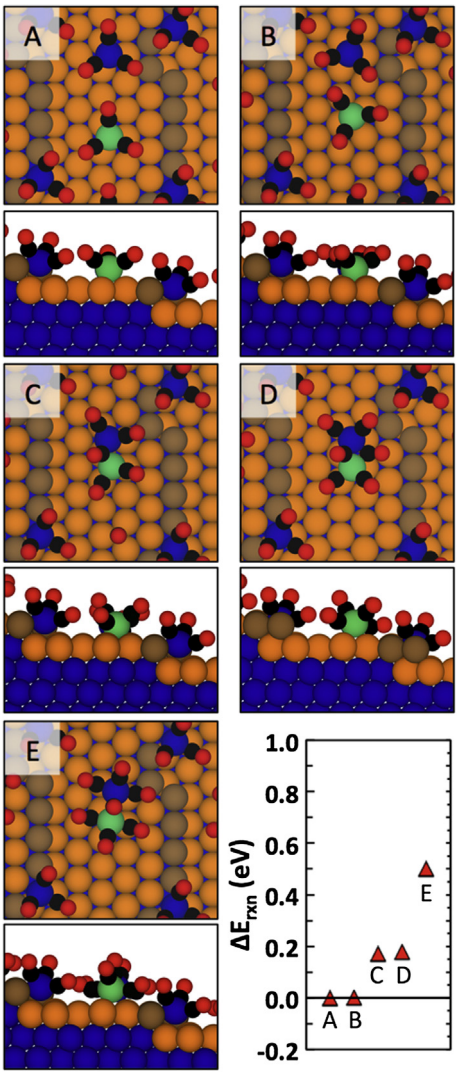

Fig. 4. Structures (A–-E) and relative DFT energy differences (lower right graph) of Co tricarbonyl dimerization reaction steps. All energy values are relative to structure (A). Two stable states, (A) and (B), are found as two Co tricarbonyl diffuse toward each other. Three possible final states are found depending on the number of CO adsorbed to the dicobalt complex: (C) pentacarbonyl, (D) hexacarbonyl, and (E) heptacarbonyl. The color scheme is identical to that used in Figs. 1 and 2 except one Co has been colored green to aid the eye.

2.6. Diffusion of $Co(CO)_3$

To explicitly show that diffusion on this surface is indeed facile, we present the minimum energy pathway (MEP) for diffusion from an (hcp) hollow site to an adjacent (fcc) hollow site on the terrace in Fig. 6. The calculation is carried out on a p(1 × 6) supercell model where a $Co(CO)_3$ species is ruptured and its corresponding kink-IS (geminal $Co(CO)_3$) reformed. The relevant diffusion pathway is set such that the initial state (IS in Fig. 6) and final state (FS in Fig. 6) stay as close as possible to the Cu/Co(1 1 1)-equivalent terrace sites. As can be seen, the diffusion MEP is remarkably shallow and a very low energy transition state (TS in Fig. 6) with an activation barrier of ~0.018 eV is found. The somewhat endothermic reaction energy (~0.015 eV) is due to either the fcc hollow site being less stable by this amount or due to the fcc hollow site interacting with the weaker (with respect to CO adsorption) terrace sites that are closer to the step edge. Since activation energy tends to decrease in value as the reaction energy decreases in value, we can say that this is likely an overestimated activation barrier, as well. Not only does this demonstrate facile diffusion of these species, but it further justifies the use of a 2-D free translator partition function for translational motion. We note that an intermediate bridge site (Br in Fig. 6) is found to be stable to within the force tolerances used (0.01 eV/Å) as well.

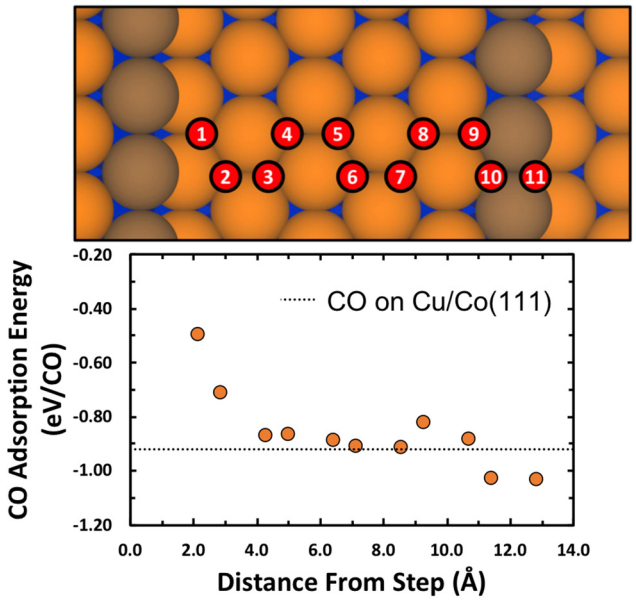

Fig. 5. CO adsorption energy on Cu/Co(7 5 5) as a function of CO distance from the step edge of the cell. These calculations were performed in the p(1 × 3) supercell. An approximate average CO adsorption energy on the Cu/Co(1 1 1) surface is shown in the graph as a dashed line, illustrating where the electronics of the Cu/Co(7 5 5) terrace converge approximately to the fcc-equivalent Cu/Co(1 1 1) surface [39]. Above the graph, the corresponding CO adsorption sites are shown. The color scheme used is identical to that in Fig. 2.

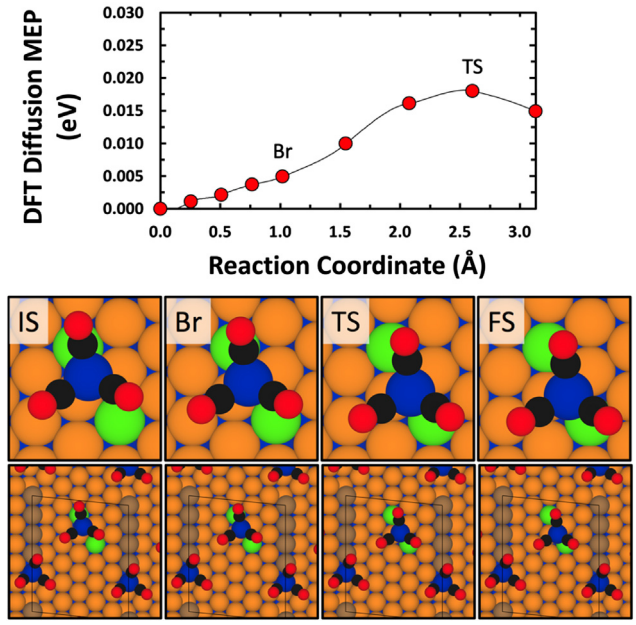

Fig. 6. Minimum energy pathway for a Co tricarbonyl diffusion across the central terrace of the Cu/Co(7 5 5) system; the corresponding structures for the labeled images are shown below the graph where "IS," "Br," "TS," and "FS" signify the initial state (an hcp hollow site), an intermediate bridge site, the transition state, and the final state (an fcc hollow site), respectively. The topmost structures are "zoomed in" compared to the bottommost structures in order to allow for a better comparison between the images. The color scheme used here is identical to that used in Fig. 2 except two Cu atoms have been colored green to help aid the eye along the diffusion pathway.

3. Summary and conclusions

With all this information in hand, we can propose a scheme for step and kink site dissolution, as shown in Fig. 7. In this snapshot, we can see that a rupturing event occurred originally at point A and subsequently induced the dissolution process that is still ongoing at point B, where the most recently ruptured kink-IS can be seen at point C. The dissolution process creates mobile Co subcarbonyls, as shown at point D (amongst others). Some of these Co subcarbonyls can dimerize, as seen at point E, or, as we envision it, even trimerize as posited at point F, and begin forming Co nanoislands with the liberation and subsequent entropy gain of additional gas phase CO thus driving further Co tricarbonyl addition and island growth. In the meantime, another geminal Co tricarbonyl could independently form at another location on the same step as at point G or on the new step as at point H, where a new geminal Co tricarbonyl ruptures and starts another dissolution process. While the exact order and structure of the catalyst shown here is speculative, we assert that the individual details that lead to this picture are well grounded in the results that were presented. In the aforementioned way, we have gained deep insights into the reconstruction mechanism experienced by a CoCu catalyst during the transient build-up of the catalytically active surface during CO hydrogenation reactions.

In conclusion, we have shown here that the formation of geminal Co tricarbonyls at step sites, predicted to occur at pressures and temperatures relevant to CO hydrogenation over CoCu catalysts, will induce the dissolution of the associated step edge. The formation of stable Co tricarbonyls is predicted to be the driving force for this process. Dicobalt subcarbonyl complex formation was shown to be feasible and suggest a route toward Co nanoisland formation: structures studied extensively in recent work [49–51]. While the ultimate fate of the Co subcarbonyls are not precisely known, the reconstruction of the catalyst is an unavoidable consequence of the process presented here as the diffusive Co tricarbonyls have the opportunity to find a stable final configuration. Such changes in aggregate would result in morphological changes of nano-sized metal particles. While the exact details involved will differ for other systems, we regard this result as a proof-of-concept for a general atomistic picture of the underlying reaction mechanism for well-known chemically-induced nanoparticle reconstruction: through low-coordinated metal site dissolution brought about by formation and diffusion of ligand-stabilized metal complexes. Given the experimental observation of similar carbonyl complexes on Ni, Ru, Rh and Co field emitter tips [23,24,31,32], and similar thiol complexes on Au surfaces [52–54], the type of process reported here may turn out to be universal across systems.

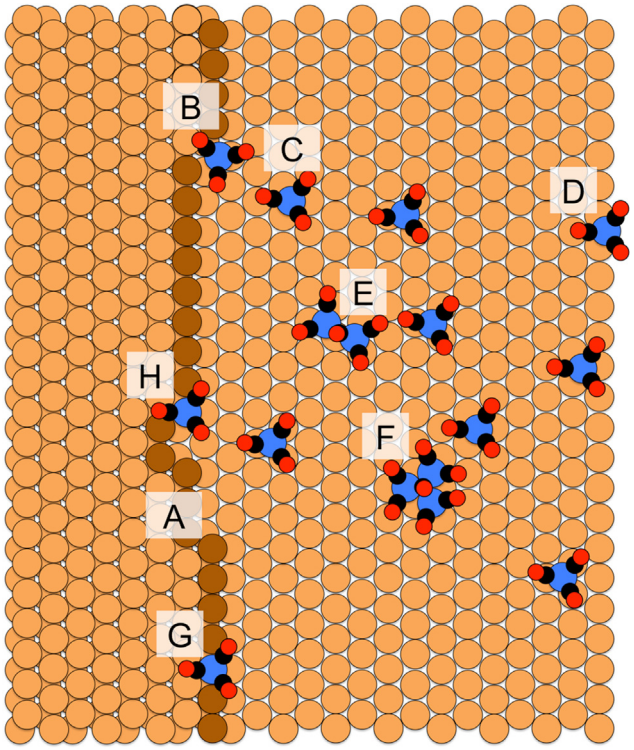

Fig. 7. A proposed scheme of the step dissolution process based on the results presented. The inset letters, A-H, are to guide the reader through the explanation of this picture in the main text. The color scheme used is identical to that used in Figs. 1 and 2.

Acknowledgements

This work was supported by the National Science Foundation under contract No. CBET-1438227 and by the National Science Foundation Graduate Research Fellowship Program under Grant No. 1347973. G.C., Seattle Chapter ARCS Fellow and NSF Graduate Research Fellow, gratefully acknowledges financial support from the Achievement Rewards for College Scientists foundation as well as the National Science Foundation Graduate Research Fellowship Program. A portion of the computer time for the computational work was performed using EMSL, a national scientific user facility sponsored by the Department of Energy's office of Biological and Environmental Research and located at PNNL. PNNL is a multi-program national laboratory operated for the U.S. DOE by Battelle. We would also like to give our sincere thanks to A.J.R. Hensley, C.J. Weststrate, and C. Stampfl for fruitful discussions and opportunities.

References

[1] H. Leidheiser, A.T. Gwathmey, The catalytic reaction of hydrogen and oxygen on plane faces of a single crystal of copper, J. Am. Chem. Soc. 70 (1948) 1200–1206, https://doi.org/10.1021/ja01183a097.
[2] R.W. McCabe, T. Pignet, L.D. Schmidt, Catalytic etching of platinum in NH_3 oxidation, J. Catal. 32 (1974) 114–126, https://doi.org/10.1016/0021-9517(74)90165-1.
[3] M. Flytzani-Stephanopoulos, S. Wong, L.D. Schmidt, Surface morphology of platinum catalysts, J. Catal. 49 (1977) 51–82, https://doi.org/10.1016/0021-9517(77)90239-1.
[4] M. Flytzani-Stephanopoulos, L.D. Schmidt, Morphology and etching processes on macroscopic metal catalysts, Prog. Surf. Sci. 9 (1979) 83–111, https://doi.org/10.1016/0079-6816(79)90001-7.
[5] P. Fenter, T. Gustafsson, Structural analysis of the Pt(110)-(1×2) surface using medium-energy ion scattering, Phys. Rev. B 38 (1988) 10197–10204, https://doi.org/10.1103/PhysRevB.38.10197.
[6] P. Fery, W. Moritz, D. Wolf, Structure determination of the (1×2) and (1×3) reconstructions of Pt(110) by low-energy electron diffraction, Phys. Rev. B 38 (1988) 7275–7286, https://doi.org/10.1103/PhysRevB.38.7275.
[7] R. Imbihl, S. Ladas, G. Ertl, The CO-induced $1 \times 2 \leftrightarrow 1 \times 1$ phase transition of Pt (110) studied by LEED and work function measurements, Surf. Sci. 206 (1988) L903–L912, https://doi.org/10.1016/0039-6028(88)90133-1.
[8] T. Gritsch, D. Coulman, R.J. Behm, G. Ertl, Mechanism of the CO-induced 1×2–>1×1 structural transformation of Pt(110), Phys. Rev. Lett. 63 (1989) 1086–1089, https://doi.org/10.1103/PhysRevLett.63.1086.
[9] T. Gritsch, D. Coulman, R.J. Behm, G. Ertl, A scanning tunneling microscopy investigation of the $1 \times 2 \rightleftharpoons 1 \times 1$ structural transformation of the Pt(110) surface, Appl. Phys. A 49 (1989) 403–406, https://doi.org/10.1007/BF00615024.
[10] J.D. Batteas, J.C. Dunphy, G.A. Somorjai, M. Salmeron, Coadsorbate induced reconstruction of a stepped Pt(111) surface by sulfur and CO: a novel surface restructuring mechanism observed by scanning tunneling microscopy, Phys. Rev. Lett. 77 (1996) 534–537, https://doi.org/10.1103/PhysRevLett.77.534.
[11] D.J. Coulman, J. Wintterlin, R.J. Behm, G. Ertl, Novel mechanism for the formation of chemisorption phases: the (2×1)O-Cu(110) "Added Row" reconstruction, Phys. Rev. Lett. 64 (1990) 1761–1764, https://doi.org/10.1103/PhysRevLett.64.1761.
[12] T. Gritsch, D. Coulman, R.J. Behm, G. Ertl, A scanning tunneling microscopy investigation of the structure of the Pt(110) and Au(110) surfaces, Surf. Sci. 257 (1991) 297–306, https://doi.org/10.1016/0039-6028(91)90800-8.
[13] M. Kiskinova, Surface structure and reactivity: reactions on face-centered cubic (110) metal surfaces involving adatom-induced reconstructions, Chem. Rev. 96 (1996) 1431–1448, https://doi.org/10.1021/cr950226y.

[14] A. Baraldi, S. Lizzit, D. Cocco, G. Comelli, G. Paolucci, R. Rosei, M. Kiskinova, Oxygen and carbon monoxide interactions on Rh(110) studied by real-time X-Ray photoemission spectroscopy, Surf. Sci. 385 (1997) 376–385, https://doi.org/10.1016/S0039-6028(97)00264-1.
[15] G. Somorjai, Surface reconstruction and catalysis, Ann. Rev. Phys. Chem. 45 (1994) 721–751, https://doi.org/10.1146/annurev.pc.45.100194.003445.
[16] B.E. Hayden, K.C. Prince, P.J. Davie, G. Paolucci, A.M. Bradshaw, Alkali metal-induced reconstruction of Ag(110), Solid State Commun. 48 (1983) 325–328, https://doi.org/10.1016/0038-1098(83)90732-9.
[17] S. Zou, R. Gómez, M.J. Weaver, Infrared spectroscopy of carbon monoxide at the ordered palladium (110)-aqueous interface: evidence for adsorbate-induced surface reconstruction, Surf. Sci. 399 (1998) 270–283, https://doi.org/10.1016/S0039-6028(97)00826-1.
[18] G. Rupprechter, T. Dellwig, H. Unterhalt, H.J. Freund, High-pressure carbon monoxide adsorption on Pt(111) revisited: a sum frequency generation study, J. Phys. Chem. B 105 (2001) 3797–3802, https://doi.org/10.1021/jp003585s.
[19] A. Gaussmann, N. Kruse, Field-ion microscopy of the CO-induced structural-changes of Pd and Pt single-crystal planes, Surf. Sci. 266 (1992) 46–50, https://doi.org/10.1016/0039-6028(92)90996-J.
[20] A. Gaussmann, N. Kruse, Real-space imaging of the CO-induced (1×2) reconstructions of Pd(011) and Pd(113), Surf. Sci. 279 (1992) 319–327, https://doi.org/10.1016/0039-6028(92)90558-N.
[21] W.A. Schmidt, J.H. Block, K.A. Becker, The topography of nickel crystals during the reaction towards $Ni(CO)_4$; a field ion microscope study, Surf. Sci. 122 (1982) 409–421, https://doi.org/10.1016/0039-6028(82)90092-9.
[22] A. Gaussmann, N. Kruse, CO-induced structural-changes of Pd particle surfaces, Catal. Lett. 10 (1991) 305–315, https://doi.org/10.1007/BF00772085.
[23] N. Kruse, A. Gaussmann, CO-induced morphological-changes of Rh crystallites - mechanisms, kinetics, and real-space imaging on the atomic-scale, J. Catal. 144 (1993) 525–543, https://doi.org/10.1006/jcat.1993.1351.
[24] D.B. Liang, G. Abend, J.H. Block, N. Kruse, Formation of nickel subcarbonyls from nickel and carbon monoxide, Surf. Sci. 126 (1983) 392–396, https://doi.org/10.1016/0039-6028(83)90733-1.
[25] N. Kruse, G. Abend, J.H. Block, Formation of Rh-subcarbonyls during the reaction of CO, CO_2 and CH_3OH with stepped Rh single-crystal surfaces, Surf. Sci. 211 (1989) 1038–1043, https://doi.org/10.1016/0039-6028(89)90872-8.
[26] M. Mihaylov, K. Hadjiivanov, H. Knözinger, Formation of $Ni(CO)_4$ during the interaction between CO and silica-supported nickel catalyst: an FTIR spectroscopic study, Catal. Lett. 76 (2001) 59–63, https://doi.org/10.1023/A:1016786023456.
[27] J.T. Yates, T.M. Duncan, S.D. Worley, R.W. Vaughan, Infrared spectra of chemisorbed CO on Rh, J. Chem. Phys. 70 (1979) 1219–1224, https://doi.org/10.1063/1.437603.
[28] F. Solymosi, M. Pasztor, An infrared study of the influence of carbon monoxide chemisorption on the topology of supported rhodium, J. Phys. Chem. 89 (1985) 4789–4793, https://doi.org/10.1021/j100268a026.
[29] M. Frank, R. Kühnemuth, M. Bäumer, H.J. Freund, Oxide-supported Rh particle structure probed with carbon monoxide, Surf. Sci. 427–428 (1999) 288–293, https://doi.org/10.1016/S0039-6028(99)00281-2.
[30] H.F.J. Van't Blik, J.B.A.D. Van Zon, T. Huizinga, J.C. Vis, D.C. Koningsberger, R. Prins, An extended X-ray absorption fine structure spectroscopy study of a highly dispersed rhodium/aluminum oxide catalyst: the influence of carbon monoxide chemisorption on the topology of rhodium, J. Phys. Chem. 87 (1983) 2264–2267, https://doi.org/10.1021/j100236a002.
[31] N. Kruse, Formation of Ru subcarbonyls by reaction of CO with stepped Ru single-crystal surfaces, Surf. Sci. 178 (1986) 820–830, https://doi.org/10.1016/0039-6028(86)90357-2.
[32] N. Kruse, J. Schweicher, A. Bundhoo, A. Frennet, T. Visart de Bocarme, Catalytic CO hydrogenation: mechanism and kinetics from chemical transients at low and atmospheric pressures, Top. Catal. 48 (2008) 145–152, https://doi.org/10.1007/s11244-008-9045-8.
[33] J. Wilson, C. de Groot, Atomic-scale restructuring in high-pressure catalysis, J. Phys. Chem. 99 (1995) 7860–7866, https://doi.org/10.1021/j100020a005.
[34] B. Eren, D. Zherebetskyy, L.L. Patera, C.H. Wu, H. Bluhm, C. Africh, L.-W. Wang, G.A. Somorjai, M. Salmeron, Activation of Cu(111) surface by decomposition into nanoclusters driven by CO adsorption, Science 351 (2016) 475, https://doi.org/10.1126/science.aad8868.
[35] R. Bliem, J.E.S. van der Hoeven, J. Hulva, J. Pavelec, O. Gamba, P.E. de Jongh, M. Schmid, P. Blaha, U. Diebold, G.S. Parkinson, Dual Role of CO in the stability of Subnano Pt clusters at the $Fe_3O_4(001)$ surface, Proc. Natl. Acad. Sci. 113 (2016) 8921, https://doi.org/10.1073/pnas.1605649113.
[36] J.Y. Park, Y. Zhang, M. Grass, T. Zhang, G.A. Somorjai, Tuning of catalytic CO oxidation by changing composition of Rh−Pt bimetallic nanoparticles, Nano Lett. 8 (2008) 673–677, https://doi.org/10.1021/nl073195i.
[37] C. Weilach, S.M. Kozlov, H.H. Holzapfel, K. Föttinger, K.M. Neyman, G. Rupprechter, Geometric arrangement of components in bimetallic PdZn/Pd (111) surfaces modified by CO adsorption: a combined study by density functional calculations, polarization-modulated infrared reflection absorption spectroscopy, and temperature-programmed desorption, J. Phys. Chem. C 116 (2012) 18768–18778, https://doi.org/10.1021/jp304556s.
[38] B. Böller, M. Ehrensperger, J. Wintterlin, In situ scanning tunneling microscopy of the dissociation of CO on Co(0001), ACS Catal. 5 (2015) 6802–6806, https://doi.org/10.1021/acscatal.5b01684.
[39] G. Collinge, Y. Xiang, R. Barbosa, J.-S. McEwen, N. Kruse, CO-Induced inversion of the layer sequence of a model CoCu catalyst, Surf. Sci. 648 (2016) 74–83, https://doi.org/10.1016/j.susc.2015.10.014.
[40] S. Carenco, A. Tuxen, M. Chintapalli, E. Pach, C. Escudero, T.D. Ewers, P. Jiang, F. Borondics, G. Thornton, A.P. Alivisatos, et al., Dealloying of cobalt from CuCo nanoparticles under syngas exposure, J. Phys. Chem. C 117 (2013) 6259–6266, https://doi.org/10.1021/jp4000297.
[41] S.K. Beaumont, S. Alayoglu, V.V. Pushkarev, Z. Liu, N. Kruse, G.A. Somorjai, Exploring surface science and restructuring in reactive atmospheres of colloidally prepared bimetallic CuNi and CuCo nanoparticles on SiO_2 *in situ* using ambient pressure X-ray photoelectron spectroscopy, Farad. Discuss. 162 (2013) 31–44, https://doi.org/10.1039/C2FD20145C.
[42] S. Alayoglu, S.K. Beaumont, G. Melaet, A.E. Lindeman, N. Musselwhite, C.J. Brooks, M.A. Marcus, J. Guo, Z. Liu, N. Kruse, et al., Surface composition changes of redox stabilized bimetallic CoCu nanoparticles supported on silica under H_2 and O_2 atmospheres and during reaction between CO_2 and H_2: *in situ* X-ray spectroscopic characterization, J. Phys. Chem. C 117 (2013) 21803–21809, https://doi.org/10.1021/jp405745n.
[43] A. Banerjee, A.P. van Bavel, H.P.C.E. Kuipers, M. Saeys, Origin of the formation of nanoislands on cobalt catalysts during Fischer-Tropsch synthesis, ACS Catal. 5 (2015) 4756–4760, https://doi.org/10.1021/acscatal.5b01169.
[44] G. Collinge, N. Kruse, J.-S. McEwen, Role of carbon monoxide in catalyst reconstruction for CO hydrogenation: first-principles study of the composition, structure, and stability of Cu/Co$(10\bar{1}2)$ as a function of CO pressure, J. Phys. Chem. C 121 (2017) 2181–2191, https://doi.org/10.1021/acs.jpcc.6b09527.
[45] J. Wellendorff, T.L. Silbaugh, D. Garcia-Pintos, J.K. Nørskov, T. Bligaard, F. Studt, C.T. Campbell, A benchmark database for adsorption bond energies to transition metal surfaces and comparison to selected DFT functionals, Surf. Sci. 640 (2015) 36–44, https://doi.org/10.1016/j.susc.2015.03.023.
[46] G.T.K.K. Gunasooriya, A.P. van Bavel, H.P.C.E. Kuipers, M. Saeys, CO adsorption on cobalt: prediction of stable surface phases, Surf. Sci. 642 (2015) L6–L10, https://doi.org/10.1023/A:1009050831597.
[47] T. Visart de Bocarmé, N. Kruse, Imaging and chemical probing on the atomic scale: reconstruction and dynamics of the systems O_2/Rh and NO_2–H_2/Pt, Top. Catal. 14 (2001) 35–42, https://doi.org/10.1016/j.susc.2015.06.024.
[48] S.H. Payne, H.J. Kreuzer, Adsorption and thermal desorption on stepped surfaces, Surf. Sci. 399 (1998) 135–159, https://doi.org/10.1016/S0039-6028(97)00737-1.
[49] E.A. Lewis, D. Le, A.D. Jewell, C.J. Murphy, T.S. Rahman, E.C.H. Sykes, Visualization of compression and spillover in a coadsorbed system: syngas on cobalt nanoparticles, ACS Nano 7 (2013) 4384–4392, https://doi.org/10.1021/nn400919y.
[50] E.A. Lewis, D. Le, A.D. Jewell, C.J. Murphy, T.S. Rahman, E.C. Sykes, Segregation of Fischer-Tropsch reactants on cobalt nanoparticle surfaces, Chem. Commun. 50 (2014) 6537–6539, https://doi.org/10.1039/C4CC01680G.
[51] E.A. Lewis, M.D. Marcinkowski, C.J. Murphy, M.L. Liriano, E.C. Sykes, Hydrogen dissociation, spillover, and desorption from Cu-supported Co nanoparticles, J. Phys. Chem. Lett. 5 (2014) 3380–3385, https://doi.org/10.1021/jz5016789.
[52] G.E. Poirier, Characterization of organosulfur molecular monolayers on Au (111) using scanning tunneling microscopy, Chem. Rev. 97 (1997) 1117–1128, https://doi.org/10.1021/cr960074m.
[53] G.E. Poirier, Mechanism of formation of Au vacancy islands in alkanethiol monolayers on Au(111), Langmuir 13 (1997) 2019–2026, https://doi.org/10.1021/la960777z.
[54] P. Maksymovych, D.C. Sorescu, J.T. Yates, Gold-adatom-mediated bonding in self-assembled short-chain alkanethiolate species on the Au(111) Surface, Phys. Rev. Lett. 97 (2006) 146103, https://doi.org/10.1103/PhysRevLett.97.146103.